

MICROMAGNETIC SIMULATIONS AND APPLICATIONS

T. Schrefl, D. Suess, H. Forster, V. Tsiantos, W. Scholz, J. Fidler, R. Dittrich

Institute of Applied and Technical Physics, Vienna University of Technology,
Wiedner Hauptstrasse 8-10/137, A-1040 Vienna, Austria

1 SUMMARY

Fast and coherent switching of small magnetic nanoparticles forms the basis of many modern magnetic devices such as ultra high magnetic storage media and precise magnetic sensors. The transition from uniform to nonuniform magnetization reversal modes is described analyzing the change of the total energy with the external field. The dynamic response of the magnetization follows from the Gilbert equation of motion which is solved numerically using a finite element method. Examples of dynamic magnetization processes are given for magnetic nanostructures as used in discrete storage media and magnetic field sensors. Both, the switching field and the switching time of Co-nanoelements decrease with increasing surface roughness of the nanostructures. In square NiFe elements two different reversal modes are observed in the simulations, depending on the domain structure for zero applied field. The field required to switch the magnetization of the C-state is about twice as large as the switching field of the S-state. Adaptive meshing is used to calculate domain wall motion in magnetic nanowires. The domain wall structure changes from a transverse wall to a vortex wall the wire diameter is increased from 20 nm to 40 nm. For a given external field, the vortex wall moves faster than the transverse wall, reaching a domain wall velocity in the order of 1000 m/s.

2 INTRODUCTION

The development of advanced magnetic materials requires a precise understanding of the magnetic behavior. A prominent example are magnetic recording systems with an areal density exceeding 100 Gbit/in², where both recording medium and recording heads have to meet certain characteristics [1]. Novel recording concepts like discrete media rely on narrow distribution of the switching field of individual magnetic island [2]. Magnetic sensors require a reproducible magnetic domain structure and a well-defined switching field of the individual magnetic elements [3]. As the size of the magnetic components approach the nanometer regime, detailed predictions of the magnetic properties becomes possible using micromagnetic simulations. The theory of micromagnetism combines Maxwell's equations for the magnetic field with an equation of motion describing the time evolution of the magnetization. The local arrangement of the magnetic moments follows from the complex interaction between intrinsic magnetic properties such as the magnetocrystalline anisotropy and the physical/chemical microstructure of the material. The finite element method is a highly flexible tool to describe magnetization processes, since it is possible to incorporate the physical grain structure and intergranular phases and to adjust the finite element mesh according to the local magnetization [4,5]. The comparison of simulations and experiments

can provide useful hints for artificial structuring of the material, in order to tailor the magnetic properties according to their specific applications [6].

The investigation of the switching behavior has been the subject of recent experimental work. In-situ domain observation using Lorentz electron microscopy [7], magnetic force microscopy [8], and time resolved magnetic imaging [9] provides a detailed understanding domain formation and reversal processes. Complementary to magnetic imaging, micromagnetic simulations reveal the physical mechanism that causes a specific switching processes. This paper reviews the basic micromagnetic and numerical background of finite element micromagnetic simulations in section 3. Section 4 presents numerical results on the switching properties of magnetic nanoelements as used for discrete storage media or magnetic sensor elements. Both the switching field and the reversal time were found to depend on the surface roughness and the granular structure of elongated Co-elements. The reversal mode of rectangular NiFe elements were found to depend on the remanent magnetic state. Finally, an adaptive mesh algorithm is applied to treat the motion of domain walls in magnetic nanowires. The magnetization distribution within the domain wall depends on the wire diameter which in turn influence the domain wall velocity.

3 MICROMAGNETICS

3.1 Basics principles

The basic concept of micromagnetism is to replace the atomic magnetic moments by a continuous function of position. In a continuum theory the local direction of the magnetic moments may be described by the magnetic polarization vector

$$\mathbf{J}(\mathbf{r}) = \mu_0 \mathbf{M}(\mathbf{r}) = \mu_0 \mathbf{m} / V \quad (1)$$

The magnetic polarization, \mathbf{J} , is proportional to the magnetization, \mathbf{M} , which is given by the magnetic moment, \mathbf{m} , per unit volume, V . μ_0 is the magnetic permeability of vacuum. The second principle of micromagnetism treats the magnitude of the magnetization as a function of temperature only. The modulus of the magnetic polarization

$$|\mathbf{J}| = J_s(T) \quad (2)$$

is assumed to be a function of temperature and to be independent of the local magnetic field. Thus the magnetic state of the system can be uniquely described by the directions cosines, $\beta_i(\mathbf{r})$, of the magnetic polarization, $\mathbf{J} = \beta J_s$. In a metastable equilibrium state, $\beta_i(\mathbf{r})$ minimizes the total Gibbs free energy of the system.

The contributions to the total magnetic Gibbs free energy are derived from classical electrodynamics, condensed matter physics, and quantum mechanics so that the continuous expressions for the energy describe the interactions of the spins with the external field, the crystal lattice, and the interactions of the spins with one another. The latter consists of long-range magnetostatic interactions and short-range quantum-mechanical exchange interactions. The competitive effects of the micromagnetic energy contributions upon minimization determine the equilibrium distribution of the magnetization. The minimization of the ferromagnetic exchange energy aligns the magnetic moments parallel to each other, whereas the minimization of the magnetostatic energy favors the existence of magnetic domains. The magnetocrystalline anisotropy energy describes the interaction of the magnetization with the crystal lattice. Its minimization orients the magnetization preferably along certain

crystallographic directions. The minimization of the Zeeman energy of the magnetization in an external field rotates the magnetization parallel to the applied field. The total magnetic Gibbs free energy, E_t , may be written in the following form [10]:

$$E_t = \int \left\{ -\frac{1}{2} \mathbf{H}_d \cdot \mathbf{J} + A \sum_{i=1}^3 (\nabla \beta_i)^2 - K_u (\mathbf{u} \cdot \boldsymbol{\beta})^2 - \mathbf{H}_{app} \cdot \mathbf{J} \right\} dV. \quad (3)$$

In (3) the first term of the integrand is the magnetostatic energy density, the second term is the exchange energy density, the third term denotes the magnetocrystalline anisotropy density, and the last term is the Zeeman energy. The integral extends over the total volume of all magnetic particles. A , K_u , and \mathbf{u} denote the exchange constant, the uniaxial magnetocrystalline anisotropy constant, and the easy direction, respectively. The intrinsic magnetic properties A , K_u , and J_s and the spatial distribution of the easy axes can be determined experimentally. \mathbf{H}_{app} is the applied field. The demagnetizing field, \mathbf{H}_d , follows from magnetic volume charges, $\nabla \cdot \mathbf{J}$, and magnetic surface charges, $\mathbf{n} \cdot \mathbf{J}$ (\mathbf{n} denotes the unit vector normal to the surface of the magnetic particles).

3.2 Magnetization reversal modes

Traditional magnetization reversal has been discussed in the framework of the nucleation theory. The critical fields which cause an equilibrium magnetic state to change were calculated using stability analysis. In addition to the switching field these theories also revealed the reversal mode [11]. The total energy of a magnetic particle may be written in terms of the magnetization distribution. In equilibrium the total energy has a local minimum. An example is an ellipsoidal particle magnetized parallel to its long axis. An oblique applied external field changes the energy surface changes, moving the position of the local minimum. As a consequence the magnetization rotates towards its new equilibrium position. At a critical value of the external field, the local minimum vanishes. The second derivative of the energy becomes zero. The magnetization configuration becomes unstable and the magnetization switches into a reversed state which is again a local minimum of the energy. The interplay between the ferromagnetic exchange energy and magnetostatic energy determines the magnetization reversal mode. A uniform magnetization throughout the particle keeps the ferromagnetic exchange energy low but causes magnetic surface charges which in turn increase the magnetostatic energy. In order to avoid magnetic surface charges the magnetization has to lie parallel to the surface. This leads to a nonuniform magnetic state which increases the exchange energy. In small magnetic particles the ferromagnetic exchange interactions keeps the magnetic moments parallel to each other and the particles reverse uniformly. During uniform rotation of the magnetization becomes aligned normal to the long axis of the particle increasing the magnetostatic energy. In larger particles the magnetostatic energy becomes important. When the magnetization may become arranged inhomogeneously without a significant expense of exchange energy, nonuniform magnetization reversal is energetically more favorable. Therefore, magnetization curling is the preferred reversal mode, if the diameter of the particle exceeds a critical length, d_{crit} . The curling mode avoids the creation of additional surface charges during magnetization reversal. Uniform rotation occurs below the critical diameter, d_{crit} , which is typically in the range of 20 nm to 30 nm. This value is significantly smaller than the single domain size, D . If a particle is smaller than D , the single domain state has a lower energy than a multidomain state for zero external field.

For application in sensor and storage elements magnetic particles should be single domain. The particle is in one of two possible metastable states and thus can store information. The preferred reversal mode is not necessarily uniform rotation and depends on the application.

Uniform rotation is favorable in magnetic sensors [12], as the rotation is reversible and thus the magnetization angle is a measure of the strength or direction of the applied field. Fast switching of the magnetization between the two metastable states is one of the prerequisites of magnetic storage elements [13]. Whether uniform or nonuniform reversal or inhomogeneous switching has a lower switching time depends on various parameters like the shape of the particle and the intrinsic damping mechanisms.

3.3 Magnetization dynamics

The dynamic response of a magnetic particle subject to an applied field follows from the Gilbert equation of motion [14]

$$\frac{\partial \mathbf{J}}{\partial t} = -\gamma |\mathbf{J}| \mathbf{J} \times \mathbf{H}_{\text{eff}} + \frac{\alpha}{J_s} \mathbf{J} \times \frac{\partial \mathbf{J}}{\partial t}, \quad (4)$$

where γ is the gyromagnetic ratio and α is a dimensionless damping parameter. The effective field, \mathbf{H}_{eff} , is the sum of the demagnetizing field, the exchange field, the anisotropy field, and the applied field. The effective field can be calculated from the variational derivative of the total Gibbs free energy

$$\mathbf{H}_{\text{eff}} = -\frac{\delta E_t}{\delta \mathbf{H}_{\text{eff}}}. \quad (5)$$

The first term of the right hand side of (4) describes the gyromagnetic precession of the magnetization around the effective field. The second term is a viscous damping term which rotates the magnetic polarization vector parallel to the field.

3.4 Numerical methods

We apply the finite element method and backward differentiation scheme to discretize the partial differential equation (4). First, the magnetic particles are subdivided into tetrahedral finite elements. Within each element we interpolate the magnetization cosines, $\beta_i(\mathbf{r})$, with linear functions. Then the energy functional (3) reduces to a function

$$E_t = E_t(\beta_1^1, \beta_2^1, \beta_2^N, \dots, \beta_1^N, \beta_2^N, \beta_3^N) \quad (6)$$

with the nodal values of β_i^n as unknowns. The index n runs from 1 to the total number of nodes, N , of the finite element mesh. The index i denotes the Cartesian coordinates. Then the effective field at each node can be approximated as

$$H_{\text{eff}, i}^n \approx -\frac{1}{\mu_0 |\mathbf{m}^n|} \frac{\partial E_t}{\partial \beta_i^n}, \quad (7)$$

where \mathbf{m}^n is the magnetic moment associated with node n . If assumed to be fulfilled at each node of the finite element mesh equation (4) reduces to a system $3N$ ordinary differential equations. A backward differentiation method [15] proved to be most efficient to solve this equation. The demagnetizing field is calculated from a magnetic scalar potential using a hybrid finite element / boundary element method [16].

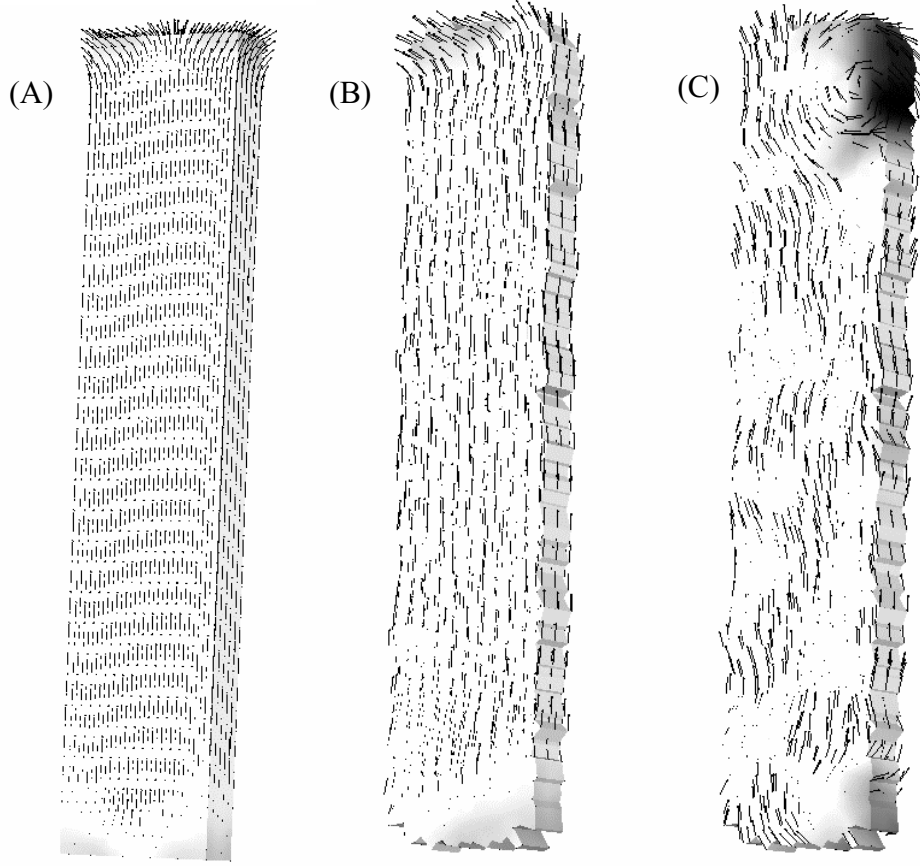


Figure 1. Co-Nanoparticles used to investigate the influence of surface roughness and grain structure on the switching field and the switching time. (A) flat surface, (B) surface roughness, (C) surface roughness and polycrystalline grains.

The finite element mesh may be adapted to the current magnetization distribution, in order to reduce the space discretization error. In order to resolve the magnetization transition in a domain wall the mesh size has to be smaller than the ferromagnetic exchange length, l_{ex} , in soft magnetic materials or the Bloch parameter, δ_0 , in hard magnetic materials. These critical length scales are given by the ratio of the exchange energy to the magnetostatic energy or the ratio of the exchange energy to the magnetocrystalline energy, respectively

$$l_{\text{ex}} = \sqrt{\frac{2\mu_0 A}{J_s^2}}, \quad (8)$$

$$\delta_0 = \sqrt{\frac{A}{K_u}}. \quad (9)$$

A failure to resolve the magnetization transition may result in a too high switching field, as domain walls may be pinned artificially on the grid [17]. Starting from an initial mesh, we apply the following scheme to refine or coarsen the mesh. After each time step we compute local error indicators. Depending on the distribution of the error indicators one of the following three procedures are applied:

Refinement. The error indicator of at least one element exceeds a global error tolerance, ϵ . The time step is rejected. The mesh is refined in regions with a high error indicator. The previously accepted magnetization distribution is interpolated on the new nodes.

Coarsening. A certain percentage of elements shows a very small error indicator far below ϵ . The time step is rejected and the current magnetization distribution is interpolated on the initial mesh.

Proceed in time. Otherwise the time step is accepted and the time integration continues with the given grid.

The above algorithm refines the mesh in regions with non-uniform magnetization, whereas it takes out elements where the magnetization is uniform. The algorithm guarantees that the simulation proceeds in time only if the space discretization error is below a certain threshold.

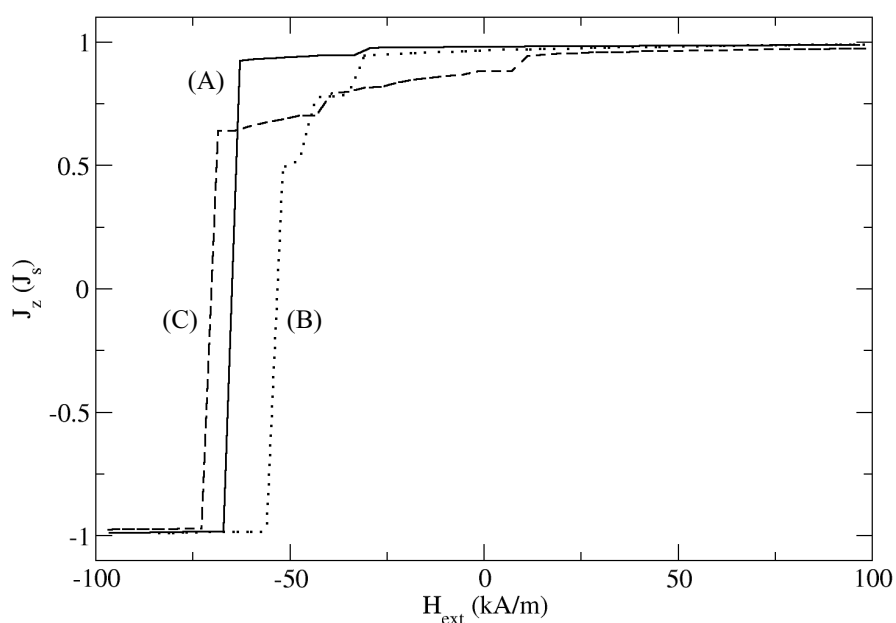


Figure 2. Calculated demagnetization curves for the three nano elements shown in figure 1. (A) flat surface, (B) surface roughness, (C) surface roughness and polycrystalline grains.

4 APPLICATIONS

4.1 Discrete media

Magnetic nanoelements may be the basic structural units of future magnetic storage media [18]. Discrete media stores each bit in an individual magnetic particle. With this technology the size of the bits, their location, and their magnetic moment are predefined, leading to high density and low signal to noise ratio. The particles are either magnetized in plane or perpendicular to the plane [2]. Here we analyze the switching behavior of elongated Co-nanoparticles which are magnetized in plane. In particular we investigate the influence of edge roughness and polycrystalline microstructure on the switching field and on the switching time. The elements are 400 nm long, 80 nm wide and 25 nm thick. We compare the magnetization reversal process in three different elements. Element (A) consists of a perfect microstructure. The surface is flat, no grains are assumed within the particle and the crystalline anisotropy is zero. Element (B) takes account of surface roughness. The notches are in average 8 nm. Element (C) consists of 500 columnar grains (diameter is 8 nm) with random distribution of the magnetocrystalline anisotropy directions. Figure 1 gives the

magnetization distribution of the three different elements for zero applied field. Figure 2 compares the calculated demagnetization curves. The external field is decreased in steps of 4.2 kA/m, in order to calculate the demagnetization curve quasistatically. For each field value the Gilbert equation is integrated until equilibrium is reached. The granular element (C) has the largest coercive field, $H_c = 72$ kA/m. The coercive field decreases by less than 10% for the perfect Co-element without crystalline anisotropy. Surface roughness leads to a reduction of the coercive field of about 20%. The switching time is studied in figure 3 which shows the time evolution of the magnetization component parallel to the external field. The field is applied instantaneously to the remanent state of the particles (figure 1). The field strength is 100 kA/m. Magnetization reversal occurs by the formation of a vortex which breaks away from the end domains. This process is similar in the elements (A) and (B). However, surface roughness causes high local demagnetizing fields which favor the formation of the vortex. In element (C) vortices are already present for zero applied field. In addition, vortices nucleate at grain boundaries within the element. Thus the total reversal time is the smallest for element (C).

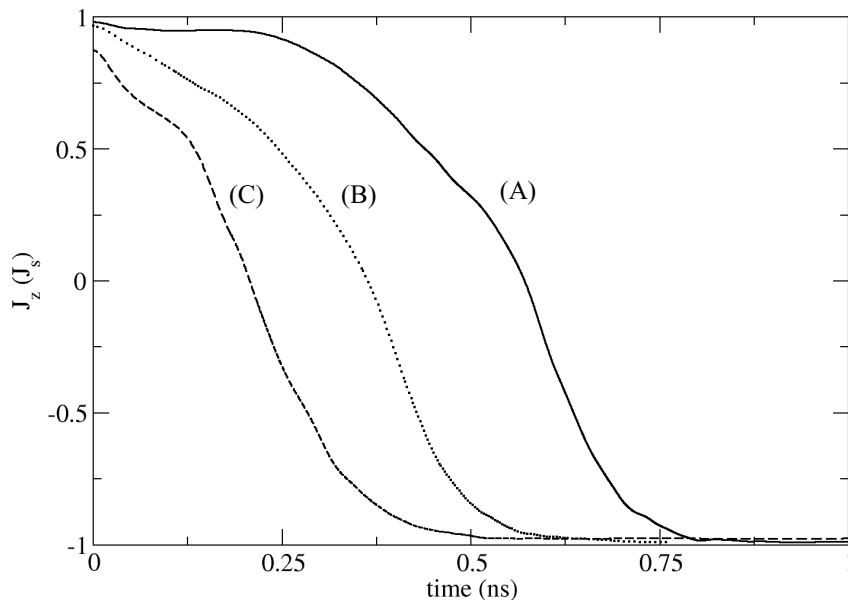


Figure 3. Time evolution of the magnetic polarization after the application of a field of $H_{app} = 100$ kA/m for the three different elements (A), (B) and (C).

4.2 Sensor elements

Magnetic multilayer films which show electron-spin dependent transport are used in sensing and storage devices. A promising system for application in magnetic random access memory or precise field sensors are spin-tunnel junctions [19]. With decreasing lateral size of the elements the uniformity of the magnetization and its influence on the tunneling behavior becomes important. Recently, Arduin and co-workers [20] investigated the magnetization reversal of the free layer using Lorentz microscopy in the transmission electron microscope. The reversal of square elements involves the formation of complex domain structures which differ significantly according to the direction in which the field is applied. A very similar structures was used in the finite element simulations. The model consists of a free NiFe layer with a thickness of 10 nm and an extension of 500 nm x 500 nm. The free layer is placed above the centre of a 1000 nm x 1000 nm wide pinned layer. In the calculations, the

magnetization of the pinned layer is kept aligned using a pinning field of $H_p = 36$ kA/m. The distance between the layers is 1.5 nm.

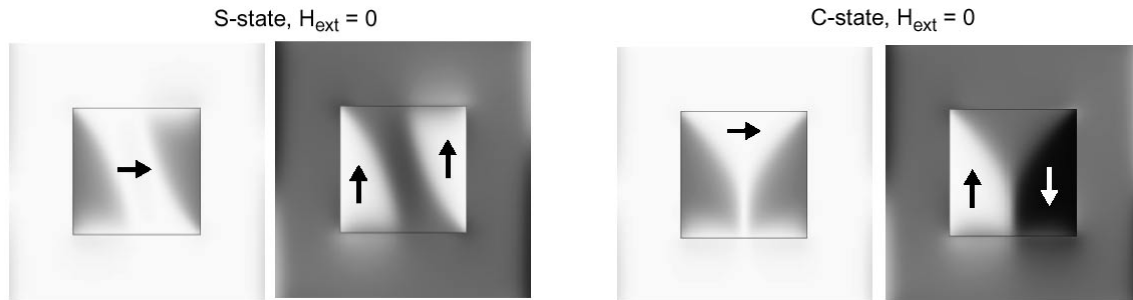


Figure 4. Magnetization configuration in the S-state and in the C-state. The gray-scale maps the magnetization component parallel (left hand side of each subfigure) and normal (right hand side of each subfigure) to the bias direction.

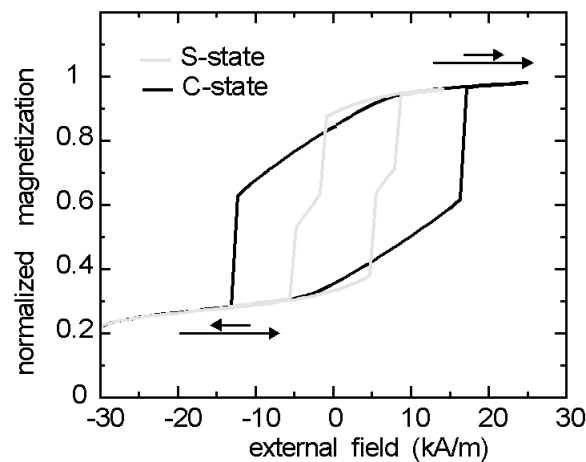


Figure 5. Free layer hysteresis loops. The calculations starts from the S-state (bright) and from the C-state (dark). The loops are shifted with respect to the origin due to the magnetostatic interactions field from the pinned layer.

The simulations reveal different equilibrium states for zero applied field depending on the magnetic history of the sample. Once a thin film element has been saturated the magnetization near the edges rotates parallel to the surface, in order to reduce the magnetostatic energy. If the magnetization in both end domains is parallel to each other the magnetization forms a “S-shape” configuration. If the magnetization along the edges is oppositely directed, the magnetization forms a “C-shape” configuration. Figure 4 gives the domain structure in the S-state and the C-state. The energy of both states differ by less than 0.2 %. The reversal process and the switching field depend on the remanent state. Once the system is in the S-state, the system will end up in an S-state after a complete magnetization cycle, although complex domain structures are formed during reversal. Similar a system being originally in the C-state will arrive in a C-state after magnetization reversal. Figure 5 shows the calculated hysteresis loops. In the free layer the end domains form in the S-state or the C-state. Starting from the S-state, the end domains grow under the influence of a reversed field. At a field of 1.6 kA/m the end domains touch each other, leading to the reversal of the centre. Finally, the residual domains along the edges parallel to the field direction reverse at a field of 5.5 kA/m. If the system is in the C-state, the growth of the end domains leads to a 4

domain flux closure structure. The domain with the magnetization in favor of the field direction expands until the free layer becomes reversed at a field of 13 kA/m. Figure 6 compares the calculated domain patterns during the magnetization reversal processes, starting from the S-state and the C-state, respectively.

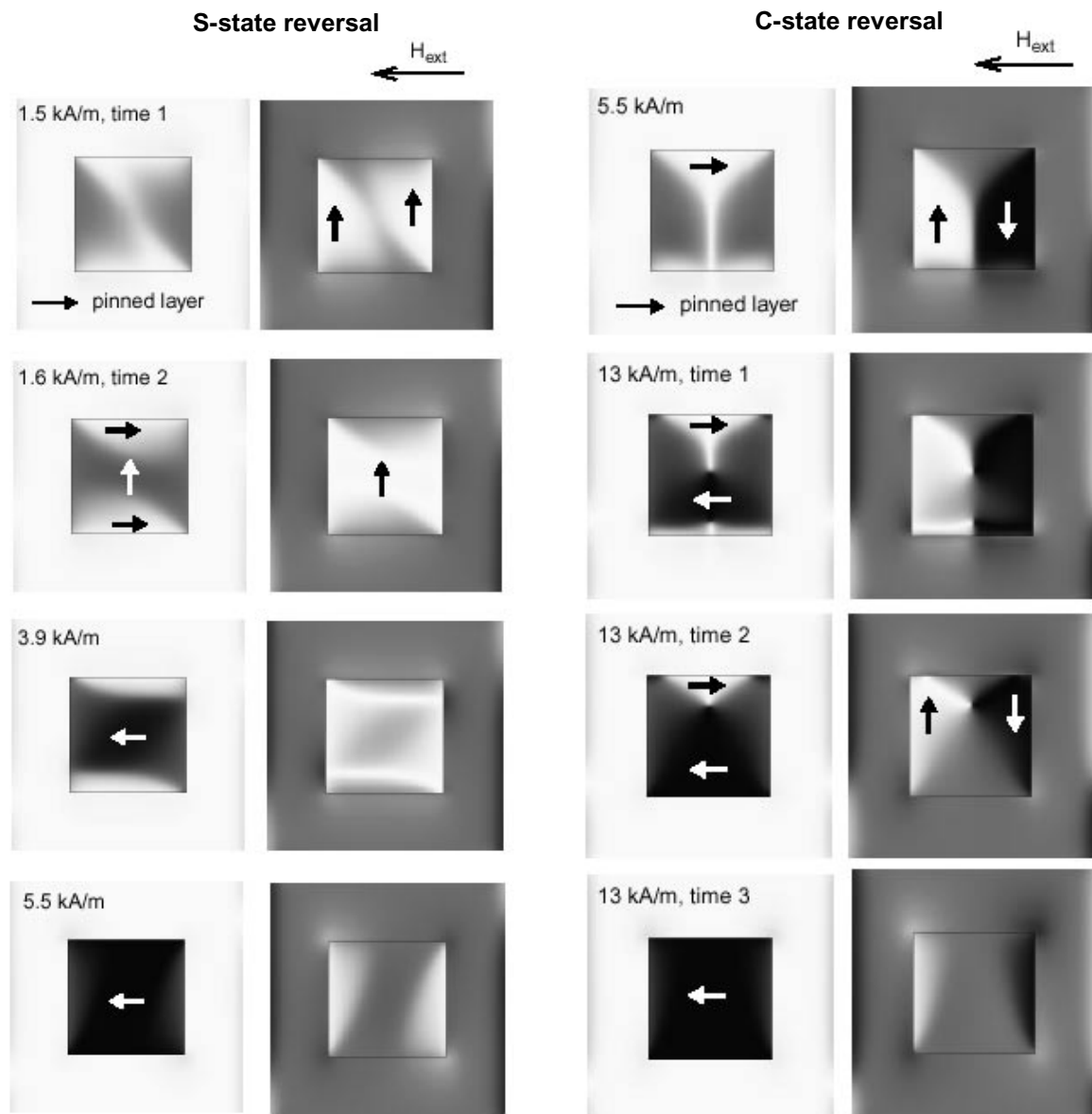


Figure 6. Left: Magnetic states during the reversal of the free layer starting from the S-state. Right: Magnetic states during the reversal of the free layer starting from the C-state.

4.3 Magnetic nanowires

Magnetic nano-wires are of great practical and theoretical interest. Future magneto-electronic devices and magnetic sensors may be based on the magneto-resistance of domain walls moving in nano-wires [21]. Here we investigate the domain wall velocity of Co nanowires as a function of the wire diameter using an adaptive algorithm which adjusts the grid to the current wall position. The thickness of the wires is varied in the range from 10 nm to 40 nm. The length of the wires is 600 nm.

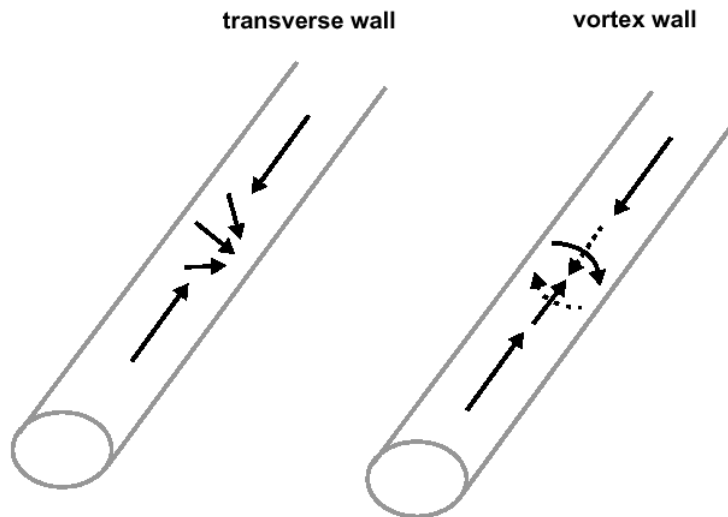


Figure 7. Schematics of the magnetization distribution in the transverse wall and in the vortex wall. The transverse wall occurs for wall diameters $d < 20$ nm and the vortex wall occurs for $d > 20$ nm.

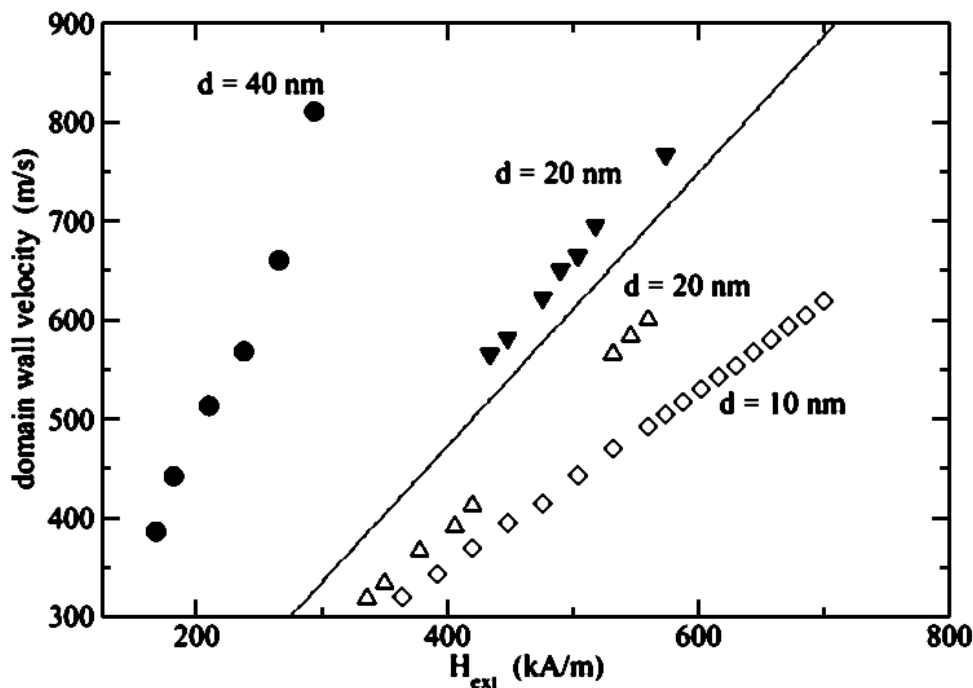


Figure 8. Domain wall velocity as a function of the applied field assuming a Gilbert damping constant $\alpha = 0.1$. The wire diameter is varied from 10 nm to 40 nm. Filled symbols: vortex wall; opaque symbols: transverse wall.

Initially, a reversed domain is created in one end. For a diameter of 10 nm a so-called transverse wall forms. In the center of the wall the magnetization points normal to the long axis of the wire. However, this configuration causes magnetic surface charges which increase the magnetostatic energy. As the wire diameter is increased the magnetization may become arranged parallel to the surface, in order to reduce the magnetostatic energy. For a diameter of 40 nm the gain in stray field energy due to the formation of a vortex is bigger than the expense of exchange energy. Thus only vortex walls are formed. For an intermediated

diameter of 20 nm both wall types occur. Figure 7 schematically shows the magnetization distribution in the transverse wall and in the vortex wall. Under the influence of an applied field the domain with the magnetization parallel to the field direction expands and the domain wall moves through the wire. The wall structure remains the same during the motion of the wall. The domain wall velocity depends on the wall structure. The vortex wall moves faster than the transverse wall. Figure 8 gives the domain wall velocity as a function of the applied field for a Gilbert damping constant $\alpha = 0.1$.

In these simulations the adaptive mesh refinement scheme described in section 3.4 was used. During wall motion the magnetization remains nearly uniform within the core of both domains. Thus it is sufficient to resolve only the magnetization transition in the domain wall and use a coarse finite element mesh within the domains. The mesh is refined at the current wall position and the finite elements are taken out again after the wall passed by. Figure 9 shows how the finite element mesh changes with time during the motion of the domain wall.

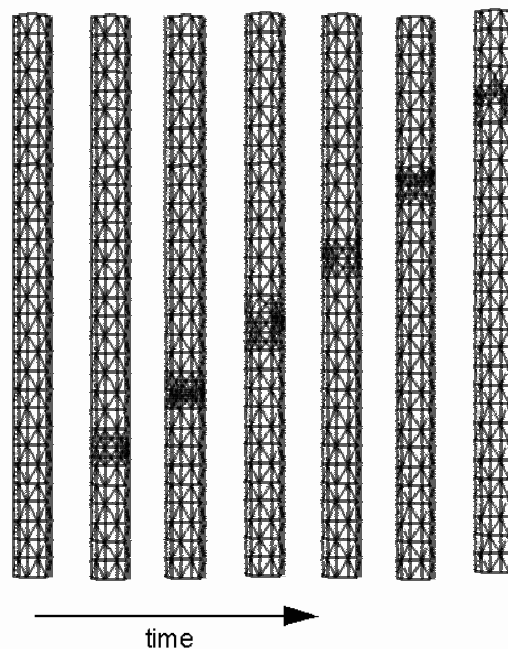


Figure 9. Sequence of meshes during the motion of a domain wall in a magnetic nanowire. The coarse mesh has a size of 20 nm. At the wall position the mesh size is about 4 nm.

5 ACKNOWLEDGMENTS

Work supported by the Austrian Science Fund (Y-132PHY, P13260-TEC).

6 REFERENCES

- [1] D.E. Speliotis, Magnetic recording beyond the first 100 years, *J. Magn. Magn. Mat.* 193, 29-35 (1999).
- [2] S.Y. Chou, Patterned magnetic nanostructures and quantized magnetic disks, *Proc. IEEE* 85, 652-671 (1997).
- [3] J.P. King, J.N. Chapman, J.C.S. Kools and M.F. Gillies, On the free layer reversal mechanism of FeMn-biased spin-valves with parallel anisotropy, *J. Phys. D: Appl. Phys.* 32, 1087-1096 (1999).
- [4] T. Schrefl, H. Forster, D. Suess, W. Scholz, V. Tsiantos and J. Fidler, Micromagnetic Simulation of Switching Events, *Advances in Solid State Physics 41*, B. Kramer (ed.), Springer, Berlin, Heidelberg, (2001) 623-635.

- [5] R. Hertel and H. Kronmüller, Adaptive finite element mesh refinement techniques in three-dimensional micromagnetic modeling, *IEEE Trans. Magn.* 34, 3922-3930 (1998).
- [6] E.D. Dahlberg, J.G. Zhu, *Micromagnetic Microscopy and Modeling*, *Physics Today* 48, 34-40 (1995).
- [7] K. J. Kirk, J. N. Chapman, C. D. W. Wilkinson, Switching fields and magnetostatic interactions of thin film magnetic nanoelements, *Appl. Phys. Lett.* 71, 539-541 (1997).
- [8] S. Ganesan, C.M. Park, K. Hattori, H.C. Park, R.L. White, H.C. Koo and R.D. Gomez, Properties of Lithographically Formed Cobalt and Cobalt Alloy Single Crystal Patterned Media, *IEEE Trans. Magn.* 36, 2987-2989 (2000).
- [9] C. H. Back, J. Heidmann, J. McCord, Time resolved Kerr microscopy: Magnetization dynamics in thin film write heads, *IEEE Trans. Magn.* 35, 637-642 (1999).
- [10] W.F. Brown, Jr, *Micromagnetics*, Wiley, New York (1963).
- [11] A. Aharoni, *Introduction to the Theory of Ferromagnetism*, Oxford University Press, New York (1996).
- [12] J.N. Chapman, P.R. Aitchison, K.J. Kirk, S. McVitie, J.C.S. Kools and M.F. Gillies, Direct observation of magnetization reversal processes in micron-sized elements of spin-valve material, *J. Appl. Phys.* 83, 5321-5325 (1998).
- [13] J.C. Mallinson, Damped Gyromagnetic Switching, *IEEE Trans. Magn.* 36, 1976-1981 (2000).
- [14] T.L. Gilbert, A Lagrangian formulation of gyromagnetic equation of the magnetization field, *Phys. Rev.* 100, 1243 (1955).
- [15] S.D. Cohen and A.C. Hindmarsh, CVODE, A Stiff/Nonstiff ODE Solver in C, *Computers in Physics* 10, 138-143 (1996).
- [16] D.R. Fredkin and T.R. Koehler, Hybrid method for computing demagnetizing fields. *IEEE Trans. Magn.* 26, 415-417 (1990).
- [17] J.M. Donahue, A variational approach to exchange energy calculations in micromagnetics, *J. Appl. Phys.* 83, 6491-6493 (1998).
- [18] J. Lohau, A. Moser, C.T. Rettner, M.E. Best and B.D. Terris, Writing and reading perpendicular magnetic recording media patterned by a focused ion beam, *Appl. Phys. Lett.* 78, 990-992 (2001).
- [19] S.S.P. Parkin, K.P. Roche, M.G. Samant, P.M. Rice, R.B. Beyers, R.E. Scheuerlein, E. J. O'Sullivan, S.L. Brown, J. Bucchigano, D.W. Abraham, Y. Lu, M. Rooks, P.L. Trouilloud, R.A. Wanner and W.J. Gallagher, Exchange-biased magnetic tunnel junctions and application to nonvolatile magnetic random access memory (invited), *J. Appl. Phys.* 85, 5828-5833 (1999).
- [20] H. Arduin, J.N. Chapman, P.R. Aitchison, M.F. Gillies, K.J. Kirk and C.D.W. Wilkinson, Magnetization reversal of patterned spin-tunnel junction material: A transmission electron microscopy study, *J. Appl. Phys.* 88, 2760-2765 (2000).
- [21] W.Y. Lee, C.C. Yao, A. Hirohata, Y.B. Xu, H.T. Leung, S.M. Gardiner, S. McPhail, B.C. Choi, D.G. Hasko, and J.A.C. Bland, Domain nucleation processes in mesoscopic Ni₈₀Fe₂₀ wire junctions, *J. Appl. Phys.* 87, 3032-3036 (2000).